Microstructural and Tribological Behavior of Pack-Borided Ni-Based Hastelloy C-276 Superalloy

YUSUF KANCA, MEHMET CAN UÇGUN, and ALI GÜNEN

Although the toughness and corrosion resistance of Ni-based superalloys are high due to their face-centered-cubic structure, their surface hardness and, thus, wear resistance are not satisfactory. The boriding process is an attempt to overcome the limitation of Ni-based superalloys in tribological applications. In this study, the boride layer was grown on Hastelloy C-276 Ni-based superalloy at 975 °C for 5 and 7 hours by powder-pack boriding to improve wear resistance. Formed boride layers were characterized using a scanning electron microscope (SEM) equipped with energy-dispersive spectroscopy (EDS), X-ray diffractometry (XRD), and nanoindentation. To investigate the effect of boride layers on the wear resistance, untreated and borided surfaces were reciprocated against an alumina ball using a pin-on-disk tribometer, at a velocity of 60 mms^{-1}, a stroke of 15 mm, a sliding distance of 300 m under loads of 5, 10, and 20 N. The results showed that the thickness of the boride layer increased at the boriding temperature elevated, which was in the range of 86.5 to 132.7 μm. The hardness of the coatings was observed to be 2016 to 2210 $HV_{0.1}$. The boriding process caused a decrease in friction coefficients by 13 to 27 pct and an increase in wear resistance by 44 to 67 times at different applied loads. As dominant wear mechanisms, untreated C-276 found abrasive wear and plastic deformation, while in the borided samples, the wear mechanisms changed to oxidation-assisted delamination. In conclusion, the boriding process improved the hardness, modulus of elasticity, and wear performance and, therefore, the service life of Hastelloy C-276.

I. INTRODUCTION

A significant material loss is reported due to the wear and corrosion damage of metals used in machinery-industry applications.[1] Heat treatment and surface-modification technologies are among the most economical and practical methods that can be used to improve wear resistance. Since wear is largely a surface-related failure, improving only the surface properties of the material is more cost effective and often offers a good solution. Of these techniques, boriding treatment is widely used in applications where high-temperature and pressure conditions are present because it provides high surface hardness and wear resistance even at service temperatures exceeding 1000 °C. Boriding is a thermo-chemical surface hardening process that has recently gained importance as it fairly lowers the friction coefficient. For instance, Hernández-Sánchez et al.[2] reported a decrease of the COF from 0.7 for AISI 316L substrate to 0.29 for the borided samples in medical applications. Therefore, the boriding process has been of interest as an alternative method for reducing wear failure experienced in various industrial applications.

In the early years of the boriding treatment, studies focused on conventional steels (carbide steels, stainless steels, tool steels, etc.), while boriding of superalloys was further introduced. The boriding process has been applied to many ferrous alloys such as structural steels, tool steels, stainless steel, and aluminum. Ni-based alloys can be also borided to obtain enhanced surface hardness and wear resistance while maintaining their corrosion resistance.[3] Compared to carburizing and nitriding, the boriding of Ni-based alloys results in homogenous surface layers with significantly high hardness. This thermo-chemical process can be categorized as paste boriding,[4–6] laser boriding,[7–9] gaseous boriding,[10] and powder-pack boriding.[11–15] Powder-pack boriding ranks the most common one among the

YUSUF KANCA and MEHMET CAN UÇGUN are with the Department of Mechanical Engineering, Faculty of Engineering, Hitit University, 19030, Çorum, Turkey. Contact e-mail: yusufkanca@hitit.edu.tr; kanca.yusuf@gmail.com ALI GÜNEN is with the Department of Metallurgy and Materials Engineering, Faculty of Engineering and Natural Sciences, Iskenderun Technical University, 31200 Hatay, Turkey.

different boring processes in terms of industrial applications.[16]

Superalloys are usually composed of various combinations of nickel, cobalt, iron, and high chromium elements and contain small amounts of molybdenum and tungsten elements which melt at high temperatures. Superalloys are known as high-temperature alloys which are mostly used at operational temperatures higher than 550 °C.[17] Ni-based superalloys exhibit superior corrosion resistance and high mechanical strength (an ultimate tensile strength of 1200 to 1600 MPa and a yield strength of 900 to 1300 MPa at room temperature). Their tensile properties do not significantly lower until 850 °C.[17–19] However, due to their ductile matrix,[12,20–23] they exhibit relatively low surface hardness (230 to 375 HV) and, thus, wear performance. Several attempts have recently been made to improve the hardness and wear resistance of Ni-based superalloys using boriding treatments. These studies obtained an enhancement in surface hardness, an increase in wear resistance, and a decrease in friction coefficients. The grown borides vary depending on the chemical composition of the substrate material and the boriding conditions (powders, temperature, and time).

Some of the literature on borided Ni-based superalloys are summarized. Sista et al.[24] applied electrochemical boriding to Inconel 600 Ni-based superalloy in a borax-based molten electrolyte bath (90 pct $Na_2B_4O_7$ + 10 pct Na_2CO_3) at 950 °C for 15 min. They found a protective boride layer of 1600 to 2100 $HV_{0.1}$ in hardness and 80 μm in thickness. The grown boride surfaces showed superior wear performance compared with the reference material in ball-on-disk wear tests which were performed under dry-sliding conditions against an alumina ball under a load of 10 N, for a sliding distance of 230 m, and at a sliding speed of 63 mms^{-1}. Deng et al.[5] paste borided the surface of Inconel 718 and observed the occurrence of the boride layers which consist of a compound layer and a diffusion zone. They conducted reciprocating ball-on-flat wear tests under 10 N at a sliding speed of 1 mm s^{-1} and reported significantly decreased wear rates and relatively lower friction coefficients after the boriding process, due to the superior hardness of the borides. Krelling et al.[14] performed pack-boriding treatment on Monel 400 using Ekabor 1-V2 boriding powder. The researchers found silicides/borides layer up to 90 μm after 6 h boriding at 900 °C, a fivefold increase in surface hardness, and an improvement in wear resistance up to 58 pct in ball-on-disk wear tests conducted at 10 N. They also reported no significant increase in layer thickness between 2 and 6 h boriding treatments because nickel-silicide layers block the further boron diffusion. Therefore, Si-free powders should be used to prevent silicide formation in boriding Ni-based superalloys.[12,25] Campos-Silva et al.[15] pack-borided Inconel 718 at 900 °C for 2 h and 950 °C for 6 h using a Si-free powder mixture of 90 pct B_4C and 10 pct KBF_4, and obtained nickel boride layers with the thickness of 19 to 50 μm and the hardness of 22.5 to 25 GPa. They carried out ball-on-plate wear experiments at a sliding speed of 30 mm s^{-1} and a sliding distance of 50 to 200 m for a

reciprocating distance of 10 mm and found an improvement in wear resistance of the substrate material by 13 to 66 times (depending on the boriding condition and the relative wear distance). Günen[12] recently pack-borided Inconel 718 at 850 °C to 1050 °C for 2 to 6 h using nano-sized B_4C powders and managed to form silicide-free boride layers, and observed that the thickness and hardness of the boride layers increased as the boriding time and temperature increased. Friction coefficients and wear rates significantly lowered after the boriding process, under dry-sliding conditions in ball-on-disk experiments at 25 °C, 400 °C, and 750 °C. Moreover, smooth and crack-free boride layers with a thickness of 22 to 86 μm and hardness of 15.57 to 18.95 GPa were obtained on Nimonic 80A by Günen et al.[11] after performing the pack-boriding process at 850 to 950 °C for 2 to 4 h using silicon-free powders. The dry-sliding wear resistance of Nimonic 80A was enhanced after the boriding process using a ball-on-disk tribometer at room temperature and 500 °C.

Hastelloy C-276, a Ni-based superalloy, has been widely used in chemical and nuclear fields such as valve parts and pumps where it is exposed to aggressive conditions, e.g., tribo-corrosive environments.[26] C-276 material maintains its durability in various corrosive environments owing to its high nickel and molybdenum contents, with the latter in particular increasing the pitting resistance of the material. In addition to corrosion resistance, wear endurance may become crucial in certain components used in chemical and nuclear industries, for instance, nozzles and pump vanes. C-276, however, has a limited wear resistance due to its low surface hardness and can often be considered unsatisfactory. Therefore, increasing the wear resistance of Hastelloy C-276 is essential to enhance its service life.

In the present study, Ni-based Hastelloy C-276 superalloy was subjected to pack-boriding treatment to enhance its surface hardness and increase its performance in tribo-corrosive environments. The boriding process was carried out at 975 °C for 5 and 7 hours using Si-free boride powders to obtain boride layers of around 100 μm. This thick layer enables a more durable surface during articulation under harsh conditions such as extreme loads and high temperatures encountered in industrial applications. The treatment temperature and duration were determined based on the literature on Ni-based superalloys. Besides, the effect of a further increase in the boriding time to 7 hours was evaluated. The primary aim was to quantify the dry-sliding wear performance of the borides grown on Hastelloy C-276 under various applied loads (5, 10, and 20 N) relative to the substrate using a pin-on-disk tribometer. This is the first attempt to the best of our knowledge. The underlying mechanisms that caused improvements in the mechanical and tribological performance on the Invar-36 surface after the boriding process was also examined using various techniques. The phase structure of the grown borides was detected by X-ray diffraction (XRD), and the microstructure of those was characterized using a scanning electron microscope (SEM) equipped with energy-dispersive spectroscopy (EDS). The hardness of the borides was measured using both

the microhardness and nanohardness techniques. The failure mechanisms developed on the wear tracks were determined using SEM–EDS.

II. MATERIALS AND METHODS

Ni-based Hastelloy C-276 superalloy used as the base material in this study was purchased from Birçelik Co. Ltd., Turkey in the plate form ($415 \times 50 \times 3$ mm^3). The chemical composition of C-276 superalloy is given in Table I, with the remaining < 0.1 wt pct consisting of other elements.

Samples of the following sizes were manufactured for the following purposes: $10 \times 10 \times 3$ mm^3 for metallographic and nanoindentation analyses, $20 \times 20 \times 3$ mm^3 for XRD analysis, and $30 \times 25 \times 3$ mm^3 for wear and friction experiments. Before the boriding treatment, the surfaces of the samples were ground with 320 to 800 grit SiC papers followed by cleaning with ethanol and distilled water. Each specimen was placed into a hermetically sealed AISI 304 stainless steel crucible packed with the boriding powders composed of 90 wt pct boron carbide (B$_4$C) and 10 wt pct sodium tetrafluoroborate (NaBF$_4$). The sealed crucible was placed in an atmospheric controlled furnace pre-conditioned to the boriding temperature. The boriding step was carried out at 975 °C for 5 hours and 7 hours. The container was taken out from the furnace after the boriding process and cooled to room temperature in the air. The specimens were removed from the cooled crucibles, and dust residues (adherent particles, *etc.*) formed on their surfaces following boriding treatment were removed by a dusting brush.

The metallographic-analysis samples were sectioned and cold-mounted. The cold-mounted sections were ground using 180, 240, 320, 400, 600, 800, 1000, 1200, and 2500 grit abrasive papers and then polished with 1 μm alumina paste. The samples were etched with a solution consisting of 70 ml H$_3$PO$_4$ and 30 ml water at 5 V for 60 s to reveal microstructural details, followed by cleaning with distilled water and drying in hot air. The phase characterization of the borides grown on Hastelloy C-276 was determined by XRD analysis. XRD patterns were recorded using a computer-controlled Panalytical Malvern Empyrean (Netherlands) X-ray diffractometer with a Cu K$_\alpha$ radiation source of a wavelength of 1.5418 Å. The scans were taken over a 2θ range from 10 to 90 deg at a speed of 1 deg min^{-1} and a step size of 0.01 deg. Metallographic studies were conducted on the polished and etched sections of the samples using a Thermo Fisher Scientific Apero S SEM–EDS. The thicknesses of grown boride and

diffusion layers were also determined using SEM and recorded as averages from 5 measurements.

Multicomponent structures of the boride layers along the cross sections were investigated using microhardness and nanoindentation techniques. Microhardness measurements were carried out using a Vickers pyramid-tip microhardness device (Q10, ATM Qness GmbH, Austria) using a 100 g load and 15 s dwell time. The nanoindentation hardness and reduced elastic modulus of the phases were measured using Hysitron TI-950 TriboIndenter (Germany) equipped with a Berkovich diamond tip. The tests were carried out under a peak load of 10 mN using a trapezoidal function (loading at a constant rate of 30 s, holding for 15 s, and unloading in 30 s). Of many analytical methods to analyze load–displacement curves obtained from nanoindentation tests,[27–29] Oliver and Pharr's method is preferred due to its common usage. Hardness and modulus of elasticity values were determined according to the Oliver and Pharr analysis method from the loading and unloading *vs* displacement curve obtained from the indentation tests.[27,30] Microhardness and nanoindentation measurements were repeated at least five and three times, respectively.

Dry-sliding wear experiments were performed on a custom-designed ball-on-plate tribometer according to ASTM G-133. The untreated and borided samples were reciprocated against a 6-mm diameter alumina abrasive ball (R$_a$ ~ 0.05 μm, hardness ~ 16 GPa). Alumina was chosen as an abrasive ball due to its inertness and high wear resistance on hard boride and carbide layers.[15] All tests were carried out at room temperature at a stroke length of 15 mm, a sliding velocity of 60 mms^{-1}, and a sliding distance of 300 m under applied loads of 5, 10, and 20 N. Each test was at least triplicated and average values $\pm$ standard deviations (SDs) were reported. During testing, the friction force was measured at 40 Hz using a 15 N load cell. The coefficient of friction (COF) was then quantified as the ratio of frictional force to test load.

Surface roughness values and wear track profiles were obtained across the worn surfaces using a 2D profilometry (MarSurf M300, Germany) based on 0.5 mms^{-1} speed and 5.6 mm scan length. 3 traces with a 5-mm gap were scanned along each wear track. At each trace, a straight line based on the unworn surface was predicted. The wear area was calculated between the predicted line and the wear track profile (see Figure 6(a)) using a customized MATLAB script, as detailed in a previous study.[31] The average area obtained from the 3 traces was multiplied by the stroke length (15 mm) to calculate the volume loss of each wear track. The wear rate (W) was subsequently calculated from the volume loss using Archard's wear equation[32,33]:

Table I. Chemical Composition (Wt Pct) of Ni-Based Hastelloy C-276 Superalloy

Material	Ni	Cr	Mo	Fe	W	Mn	V	Co	Si	Cu	Nb
C-276 [Wt Pct]	58.34	16.10	15.36	6.07	3.37	0.37	0.14	0.05	0.02	0.02	0.01

$$W = \Delta V/(F_N S), \qquad [1]$$

where ΔV: Wear track volume (mm^3), F_N: Test load (N), and S: Sliding distance (m).

A 3D profilometry (Contour GT, Bruker, Germany) was used to assess surface topographies and to confirm volume loss following wear testing. Images were stitched using a 5 × magnification objective. The failure mechanisms and the elemental distribution of the worn surfaces were examined using SEM–EDS at 10 kV.

III. RESULTS AND DISCUSSION

A. *XRD, Microstructure and Hardness Analyses*

Figure 1 shows XRD patterns obtained from borided Hastelloy C-276. Ni$_2$B (ICDD: 03-065-2691), CrB (ICDD: 01-089-3587), Fe$_2$B (ICDD: 01-075-1062), and MoB$_2$ (ICDD: 01-086-1099) phases were detected in both structures of 975 °C-5 hours and 975 °C-7 hours (indexed in Figure 1). The intense diffraction peaks reflected at the (002) plane correspond to the Ni$_2$B phase, and the lattice constant was determined as 2.1303 Å. The intense Ni$_2$B phase is associated with high Ni content present in the Hastelloy C-276 substrate. When the boriding duration increased from 5 to 7 hours, the peaks of the Ni$_2$B phase shifted from 42.39 deg to lower 2θ values (35.67 deg). In addition, the peak intensities of MoB$_2$ and CrB phases increased while those of the Fe$_2$B phase decreased. The increases in MoB$_2$ and CrB phases at higher boriding durations may affect the mechanical properties of the boride layers. This is because the hardness of these phases (24 to 27 GPa for MoB$_2$ and 19 to 23 GPa for CrB) is reported to be considerably greater than the hardness of Ni$_2$B (15 GPa).[34] However, the presence of CrB in the boride layers reduces the fracture toughness of the boride layers.[35]

Figures 2 and 3 exhibit cross-section SEM analysis of borided Hastelloy C-276 superalloy, obtained at 500 × and 1200 × magnifications. The boride layer thickness of the 975 °C-7 hours samples (132.65 μm) was observed to be greater than the thickness of 975 °C-5 hours (86.5 μm) (Figure 2). The grown borides were observed to be compact as well as porosity and microcrack free, which indicates a suitable set of boriding temperature and duration. Moreover, we noticed that the borides were successfully formed at the corners of the samples, which has a practical application. Because the boriding treatment can be used in machine parts with complex geometries such as gears, molds, valves, *etc*. The phenomena related to the non-formation of the coatings at the corners would be encountered in various techniques such as electrodeposition.

Figures 3(a) and (b) shows the existence of three distinct zones: a boride layer, the substrate, and a transition (or a diffusion) layer, as stated in the previous study conducted on Ni-based superalloy.[12] The diffusion layer acts as a bridge between the boride and substrate regions during heating and cooling processes as these regions have different thermal expansion coefficients. This layer also increases the adhesion force between the coating layer and the substrate material. Although the transition layer has been reported to be thicker than the boride layer in borided steels,[36] it has a lower thickness than the boride layer in borided superalloys.[11] This is because the alloying elements of superalloys slow down the boron diffusion and hinder the diffusion progress. Thus, using the same boriding conditions (temperature and duration), thicker boride layers and transition zones are obtained in unalloyed steels as compared to alloyed steels, stainless steels, superalloys, and high entropy alloys. Moreover, EDS analysis showed that the obtained boride layer consisted of 72.6 pct B, 18.2 pct Ni, 6.7 pct Cr, 2.0 pct Fe, and 0.4 pct W (Figure 2). As EDS spectra move from the surface towards the interior, the B ratio gradually decreases and then reaches "0" at the substrate while the concentrations of other elements which exist in the chemical structure of the substrate increase. Also, the elemental ratio of the substrate obtained from EDS analysis (Figure 3) is comparable to that supplied by the material provider (Table I).

Increasing boriding time caused an increase in the thicknesses of both the boride layer and transition zone because boriding is a diffusion-based process (a transport of atoms from high- to low-concentration regions). This is explained by Fick's first law in which diffusion flux (atomic mass perpendicular to the unit cross-sectional area of the solid per unit time) is proportional to the concentration gradient (the slope of concentration *vs* distance of diffusing atoms), which is called steady-state diffusion.[37]

The hardness values of the grown boride layers were in the range of 2016 to 2210 HV$_{0.1}$, greater than some borided Ni-based superalloys while similar to others. Günen *et al*.[22] borided Inconel 625 superalloy using three different powders (Nanobor, hBN, and Ekabor2) at 1000 °C for 3 h; using these powders, the thickness and hardness of the grown layers were reported to be 72, 63, and 23 μm and 2167, 1453, and 1750 HV, respectively. Hence, the boride phases to be obtained depend to a great extent on the boriding powders used as well as the chemical composition.

Figure 4 shows the typical load-depth curves of borided Hastelloy C-276 (975 °C-5 hours and 975 °C-7 hours). On the load–displacement curves, the initial steep slope and small recovery depth suggest high stiffness. For both boriding conditions, large variations of the residual indentation depths were observed from the surface to the interior, which indicates the distinctions in the hardness and the resistance against deformation through the substrate, diffusion, and boride layers. The hardness and modulus of elasticity of the coatings may vary according to many factors such as interatomic distance, planar density, the orientation of the crystal, grain size, grain boundary, pore structure, and residual stress.[38] In addition, the area under the loading–unloading curve, and hence, the energy dissipation for the diffusion zone was decreased from 751.4 to 576.8 μNμm (calculated using ImageJ) when the boriding duration increases from 5 to 7 hours.
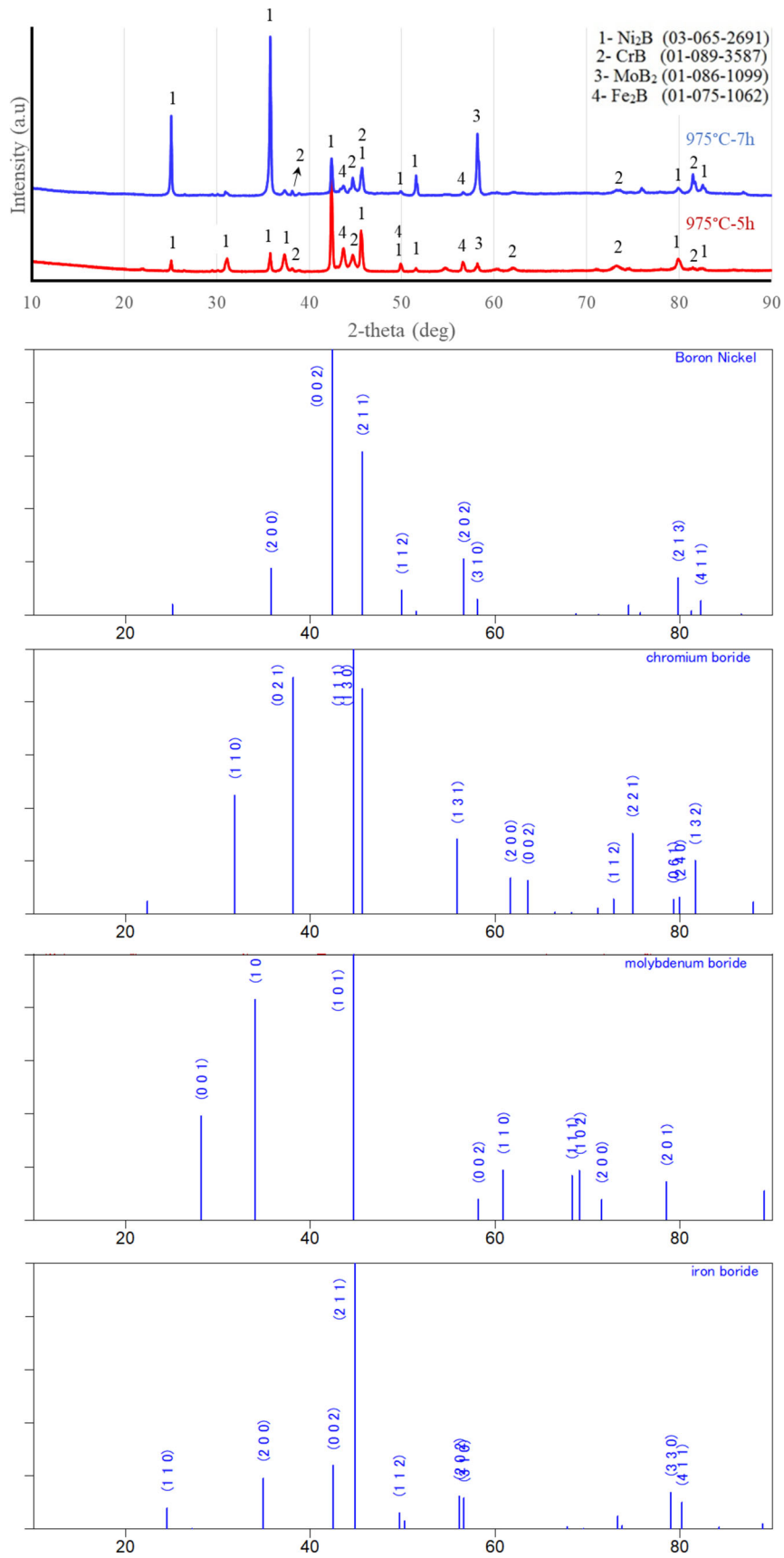
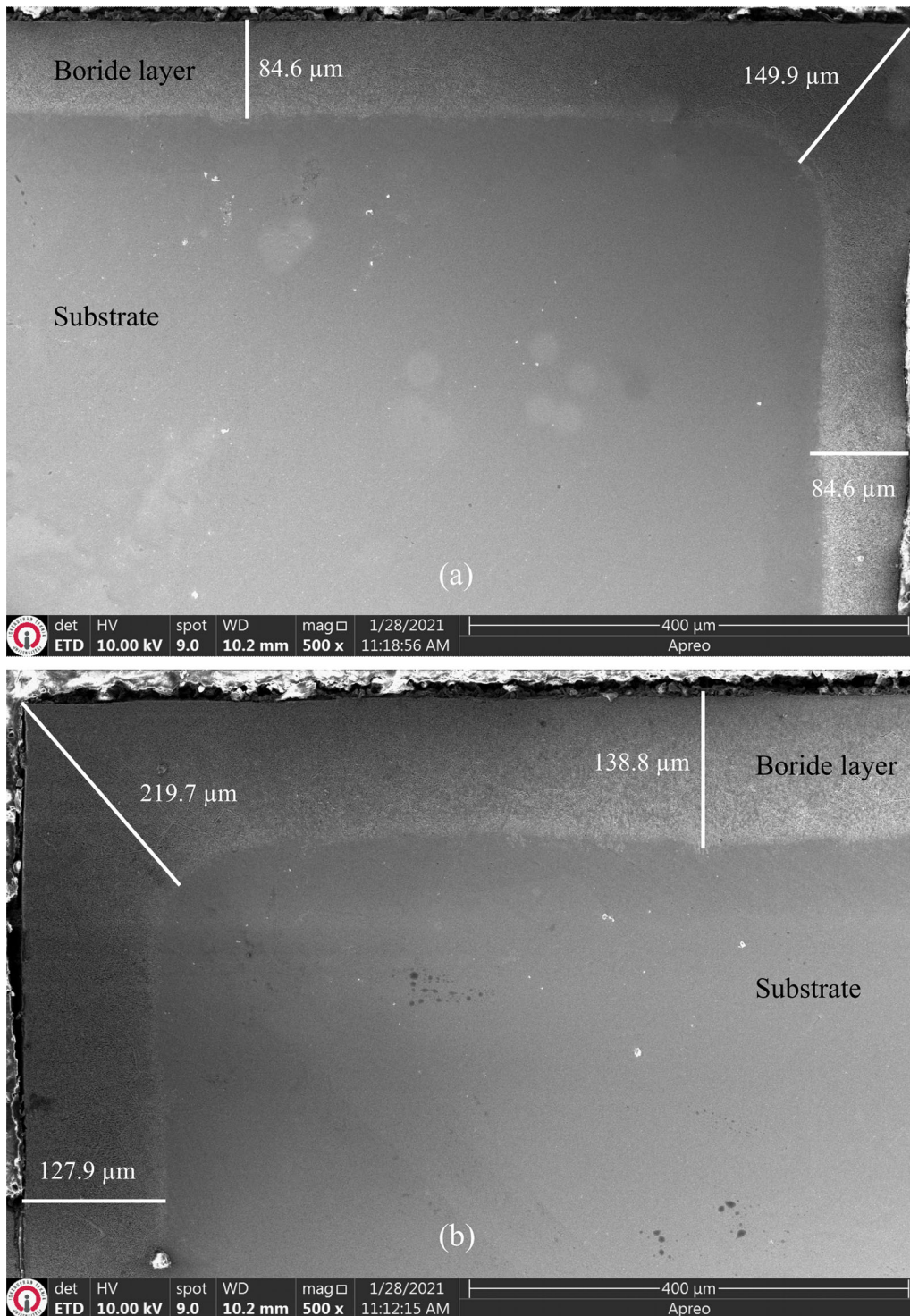Fig. 1—XRD analysis of the boride layers grown on C-276 superalloy.

Fig. 2—Cross-sectional SEM micrographs of the boride layers grown on Hastelloy C-276 surface; (*a*) 975 °C-5 h and (*b*) 975 °C-7 h. The images magnified by 500 × show the boride layer and its thickness as well as the substrate.

Nanoindentation test results are shown in Table III. The hardness values of borided Hastelloy C-276 were observed to be 24.5 to 26.0 GPa at the boride layer, 8.6 to 9.1 GPa at the transition region, and 5.9 to 6.1 GPa at the substrate. Increasing boriding time caused a small decrease in the displacement under a given load and,

thus, to a slightly harder surface. The hardness values showed a decreasing trend from the boride layer to the transition zone and to the substrate, which supports the existence of the transition zone indicated in SEM images (Figures 3(a) and (b)).

Atom %	B-K	O-K	Cr-K	Fe-K	Ni-K	Mo-L	W-M
Pt1	73.22	0.00	6.39	2.02	17.94		0.42
Pt2	74.73	0.00	6.41	1.73	16.73		0.40
Pt3	65.41	0.00	8.51	2.69	22.75		0.64
Pt4	0.00	0.50	19.53	6.81	61.51	10.26	1.39

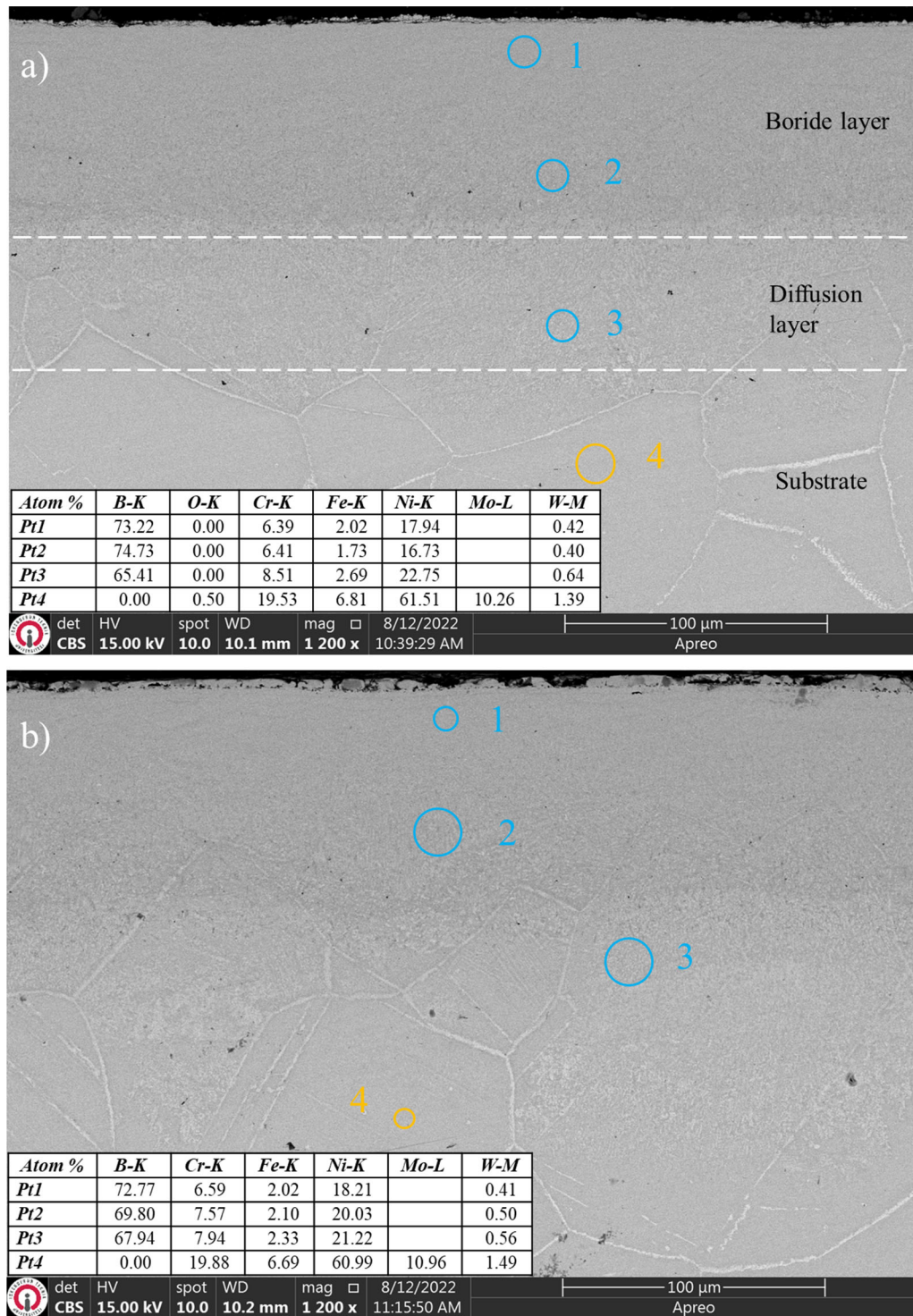| Atom %	B-K	Cr-K	Fe-K	Ni-K	Mo-L	W-M
Pt1	72.77	6.59	2.02	18.21		0.41
Pt2	69.80	7.57	2.10	20.03		0.50
Pt3	67.94	7.94	2.33	21.22		0.56
Pt4	0.00	19.88	6.69	60.99	10.96	1.49

Fig. 3—Cross-sectional SEM micrographs and EDS analysis of the boride layers grown on Hastelloy C-276 surface; (a) 975 °C-5 h and (b) 975 °C-7 h. Images were magnified by 1200×.

The measured nanohardness values were slightly greater than the microhardness values, most likely as a result of the indentation size effect.[39,40] The sharp increase in nanohardness value at a lower load is caused by the activation of local dislocation mechanisms.[41]

B. *Friction Coefficient Analysis*

The effect of the boriding process on the friction performance of Hastelloy C-276 was investigated as the untreated and borided samples were articulated against the alumina ball in dry-sliding conditions. The friction
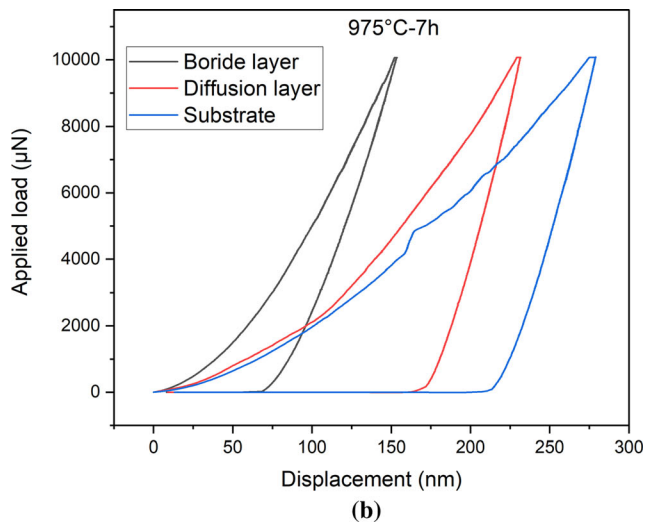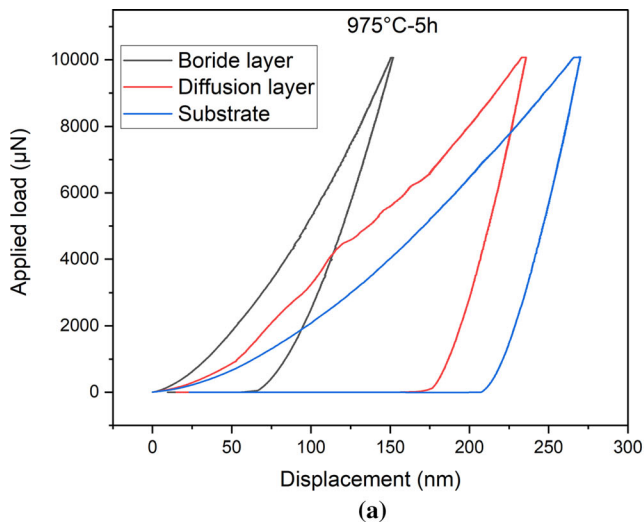
Fig. 4—Typical indentation load *vs* displacement curves were obtained from nanoindentation measurements of the borided samples: (*a*) 975 °C-5 h and (*b*) 975 °C-7 h.

coefficient (COF) was continuously recorded during the wear tests. Figures 5(a) through (c) displays the COF over time under loads of 5, 10, and 20 N.

The COF curves of both untreated and borided C-276 had a running-in stage, where the COF gradually increased to a certain value during the early stage of sliding depending on the applied load. It is thought that such friction behavior may be caused by the presence of trapped wear debris on the substrate, enabling the plowing effect, as explained in previous studies.[42,43] Experimental methods such as an atomic force microscopy can be used to quantify the plowing effect. Applying this technique, Schmid *et al.*[44,45] generated a single plow track using a sharp diamond indenter to simulate a single tool asperity on three commercial aluminum alloys. Moreover, during the initial articulation, bonding force between the rubbing surfaces increases, leading to microwelding because of progressive breakage of oxide and deposited layers on the substrate. This increased adhesion and contact temperature of the contact area may also be responsible for COF increment.[43] COF of untreated C-276 alloy was observed to stabilize after 1 min of testing at 0.61 under 5 N and at 0.59 under 10 N. When 20 N load was applied, COF equilibrium value found a slight increase in the range of 0.45 to 0.51 over testing. On the other hand, COF of borided C-276 was equilibrated after 25 min of testing at 0.46 to 0.50 under 5 N and after 20 min at 0.42 to 0.47 under 10 N. The small increases in the COF equilibrium values should be noted. At 20 N, the COF reached a stable value of 0.43 for 975 °C-5 hours while that of 0.36 for 975 °C-7 hours after 15 minutes of testing. Also, there were found to be fluctuations in the COF, which decreased as the applied load increased.

Figure 5(d) shows the average COF of each tested material against the applied load. At all loading conditions, borided C-276 (0.35 ± 0.03 to 0.47 ± 0.05) provided lower average COF than untreated C-276 (0.48 ± 0.01 to 0.61 ± 0.01). The highest average COF was obtained from the untreated samples worn at 5 N while the lowest average COF was obtained from the 975 °C-5 hours samples worn at 20 N. The boriding process decreased mean COF values by 23 to 26 pct under 5 N, ~ 27 pct under 10 N, and 13 to 27 pct under 20 N. The variation in average COF was due to the boriding condition – 975 °C-7 hours generally found a higher reduction rate in average COF as compared to 975 °C-5 hours. The increased COF of untreated C-276 superalloy could be caused by compaction and adhesion of wear debris on the surface due to heavy plastic deformation (Figure 9), which restrains the sliding of the abrasive ball against the sample.[5,46] Mean COFs of both untreated and borided C-276 significantly decreased as the applied load increased, consistent with the literature on Ni-based superalloys.[47,48] This may have arisen from the occurrence of higher oxidation at elevated loads (Figures 10 and 11) due to an increased contact temperature, as suggested by Chowdhury *et al.*[43] Moreover, the decrease of the contact area due to a large amount of trapped wear debris between the rubbing surfaces at higher applied loads (Figure 9(c-2)) are also believed to be responsible for the decrease in the COF.[49,50]

C. Dry-Sliding Wear Analysis

Figure 6 shows typical wear profiles of untreated and borided Hastelloy C-276 superalloy, obtained across the wear tracks at loads of 5, 10, and 20 N using a 2D profilometry. The boriding process resulted in reducing the dimensions (widths and depths) of the wear track profile at any given load (Figure 6 and Table IV). Moreover, the dimensions of the wear tracks increased at higher applied loads for both untreated and borided Hastelloy C-276. For instance, the wear track depth of borided Hastelloy C-276 (1.8 to 7.9 μm) was significantly lower than that of untreated C-276 (58.1 to
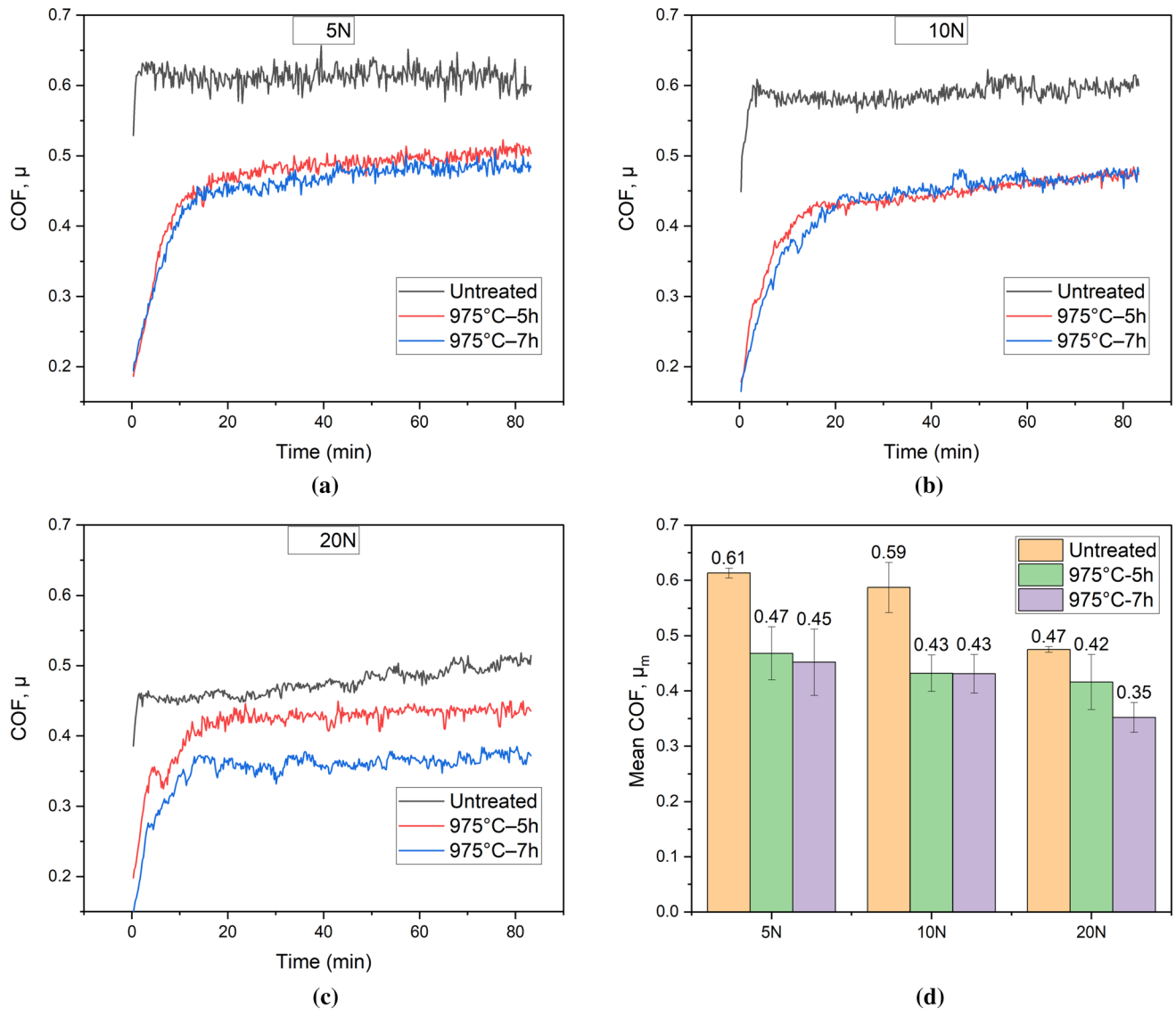
Fig. 5—Friction coefficient (μ) over time under the applied loads of (*a*) 5 N, (*b*) 10 N, (*c*) 20 N, obtained during the articulation of alumina ball against untreated and borided Hastelloy C-276; (*d*) variation of average friction coefficient (μ_{m}) against the normal load (mean ± SD, n ≥ 3).

92.6 μm). The presence of piled wear debris (extrusions) (Figure 6(a)) at the edges of the wear marks indicates that more severe deformation occurred in the untreated samples.

While the wear traces of untreated Hastelloy C-276 appear in a semi-ellipse structure (Figure 6(a)), a zigzag-shaped wear profile was observed on the borided samples (Figure 6(b) and (c)). The phases grown on a substrate may have various hardness values – relatively softer phases are more prone to damage when the surface is articulated against an abrasive ball. This phenomenon causes the occurrence of localized fractures on the worn surfaces, and thus, the formation of irregular wear morphology,[51] which was even more distinct at elevated loads (Figure 6(b) and (c)). It could also be speculated that the hard phases grown at the boride layers would cause surface damage on the

abrasive counterpart, which may trigger the irregular wear profiles of the borided C-276 superalloy.

The variations of the volume loss for the untreated and borided samples, calculated by multiplying the average area loss of a wear track by its length, are shown in Figure 7(a). The borided specimens provided a better wear response against the abrasive ball than the untreated samples at all loading conditions. This can be attributed to the higher hardness and modulus of elasticity of Hastelloy C-276 obtained after the boriding treatment (Tables II and III).[52] Following the boriding process, the volume loss decreased from 0.94 to 0.018 mm³ at 5 N, from 1.3 to 0.019 mm³ at 10 N, and from 1.9 to 0.042 mm³ at 20 N. The improvement in wear resistance at 20 N (44 times) was lower than that at 5 N (51 times) and 10 N (67 times), probably because ceramic-based borides are more prone to fracture
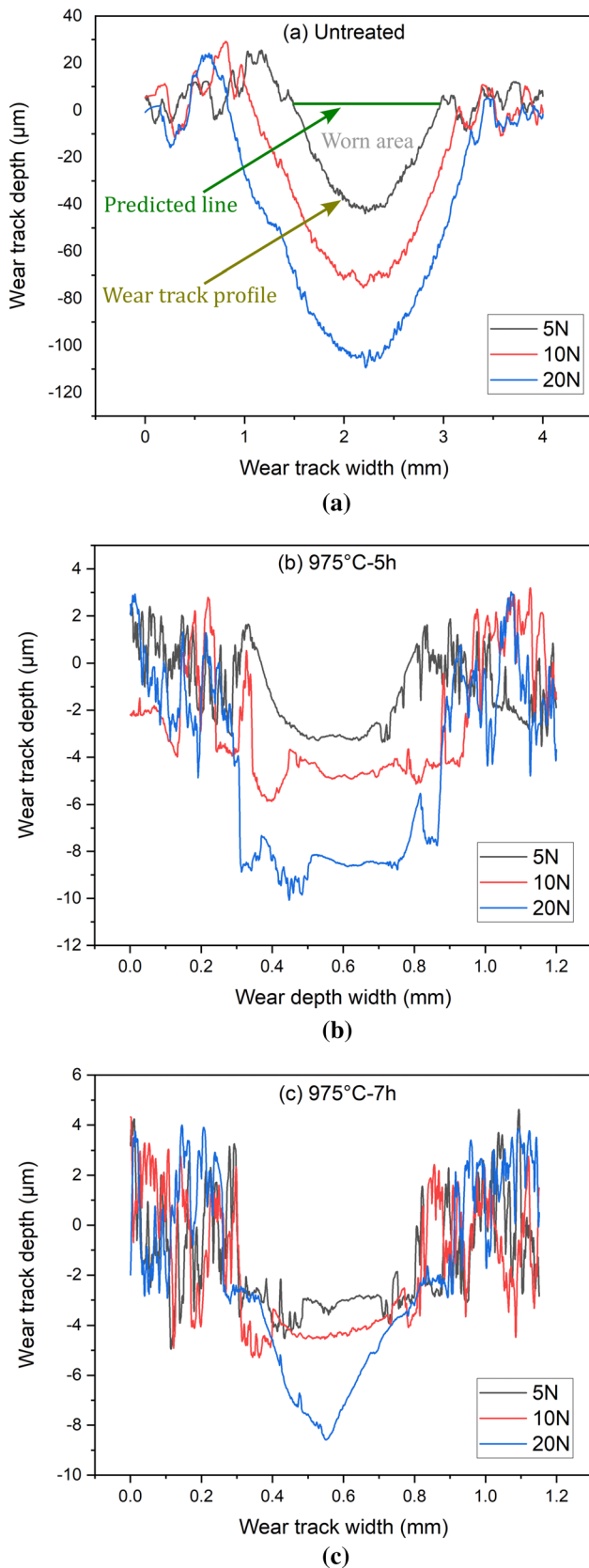
◄ Fig. 6—2D wear track profiles of (*a*) untreated, (*b*) 975 °C-5 h, and (*c*) 975 °C-7 h Hastelloy C-276, exposed to wear tests at 5, 10, and 20 N. Note that the worn area (between the wear track profile and the predicted line based on the unworn surface) is highlighted, which is used to calculate the volume loss on a slice-by-slice basis.

(Figures 10(c-2) and 11(c-2)) at increased loads and, thus, pressures due to their brittle structure.[53–55] The worn particles entrapped between the articulating surfaces during the wear tests may further contribute to the increased volume loss of the material.[22] Moreover, the boriding time (5 and 7 hours) did not cause a considerable alteration in the wear performance of Hastelloy C-276. This is mainly because the wear track depth of the borided samples (1.8 to 7.9 μm) (Figures 6(b) and (c)) was only a limited part of the grown boride layers (86.5 to 132.7 μm) (Figure 2 and Table II). So, the lower sides of the borides were not exposed to the wear process. On the other hand, Campos-Silva *et al.*[15] pack-borided Inconel 718 superalloy at 900 °C for 2 h and 950 °C for 6 h and reported that the latter provides increased wear resistance by two and threefold because its wear depth exceeds the boride layers.

Figure 7(b) shows the relationship between the specific wear rates, calculated using Eq. [1], and normal loads. After the boriding process, the wear rates were significantly decreased to 1.9, 1.4, and 2.2 pct of the untreated samples at loads of 5, 10, and 20 N, respectively. Additionally, a higher applied load led to a lower specific wear rate for all materials. For instance, the specific wear rate of 975 °C-7 hours was about 1.5 × 10^{-5} mm^3/Nm at an applied load of 5 N, which decreased to 0.77 × 10^{-5} mm^3/Nm at 10 N. A continuous decrease in the specific wear rate (0.55 × 10^{-5} mm^3/Nm) was still observed as the applied load further increased to 20 N. Wear rates and volume losses were found to be inversely proportional, as reported previously.[56] The tendency of the specific wear rate against normal load in Figure 7(b) is in line with a previous study.[42] The decreasing trend in wear rate may be attributed to the compaction of wear particles detached from the worn surface at increasing applied load.[46,56] In addition, increasing contact temperature obtained at higher applied loads between the articulating surfaces would lead to the formation of a tribo-oxide layer on the worn surfaces (Figures 9, 10, and 11). The presence of oxides on the sample surface acts as a lubricant significantly reducing wear rates.[57,58]

Arithmetical mean roughness (R$_a$) values obtained from the unworn and worn surfaces of the untreated and borided Hastelloy C-276 samples are given in Tables II and IV, respectively. The surface roughness was found to decrease after wear testing for all test groups. As the worn surfaces were compared, the R$_a$ of the untreated samples was generally found to be greater than that of the borided ones. Furthermore, increasing load caused an increase in the R$_a$ values of the untreated samples (designated as severe damage) but a decrease in those of the borided samples, which is attributed to increased occurrence of glazed layer.
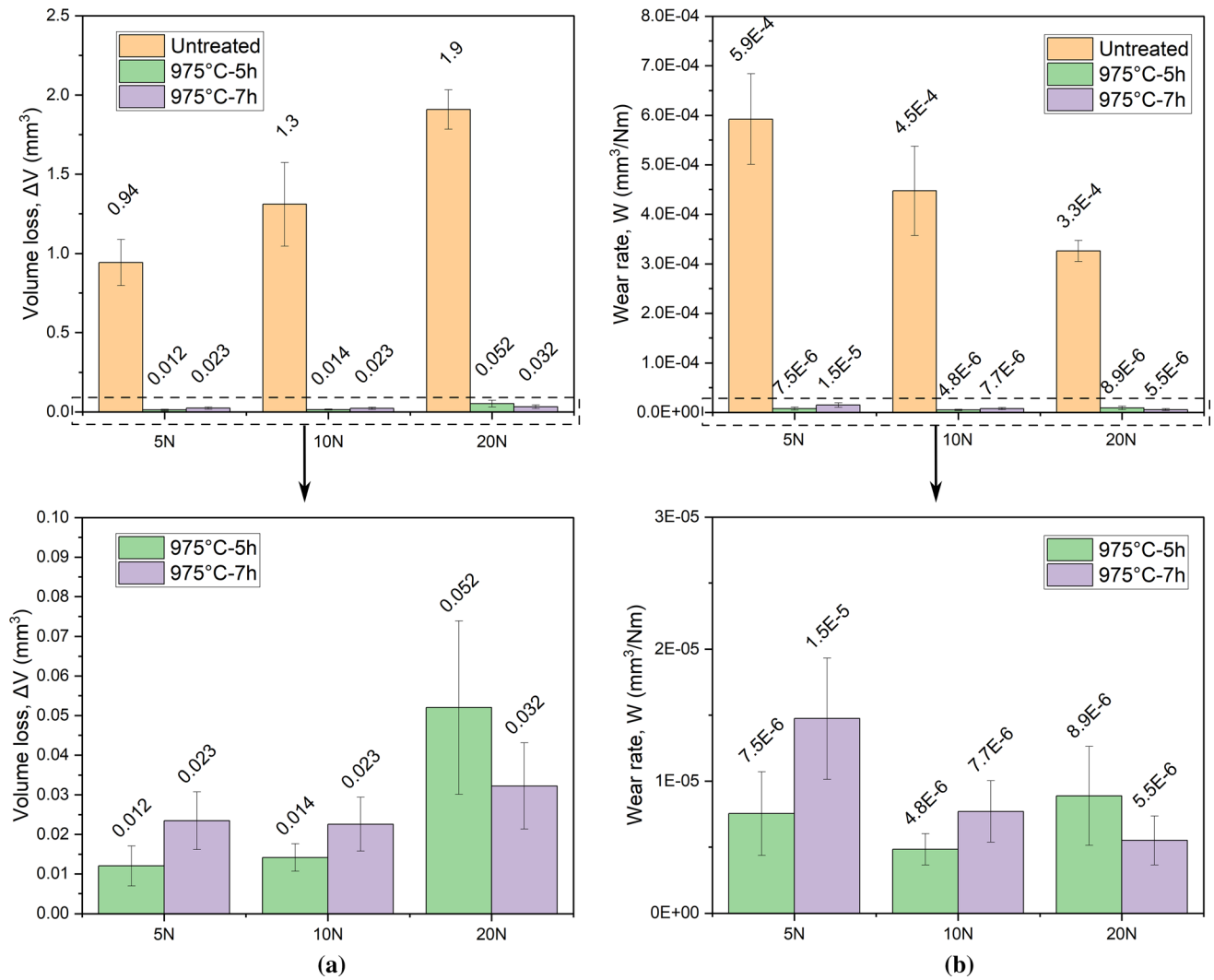
Fig. 7—(a) Volume loss and (b) wear rate of the samples subjected to the wear experiments at 5, 10, and 20 N (mean ± SD, n ≥ 3). The upper plots have greater ranges to show the higher and lower values together. The lower plots show data from only the borided samples at higher magnification.

Table II. Some Characteristics of Untreated and Borided Hastelloy C-276 (Mean± SD, n ≥ 3)

Sample	Boride Layer Thickness (μm)	Diffusion Region Thickness (μm)	Microhardness ($HV_{0.1}$)	Surface roughness (R_a, μm)
Untreated	—	—	250 ± 10	0.601 ± 0.074
975 °C-5 h	86.5 ± 1.6	49.3 ± 11.7	2016 ± 125	0.537 ± 0.161
975 °C-7 h	132.7 ± 5.6	65.2 ± 10.3	2210 ± 130	0.948 ± 0.075

To better understand the change in the wear performance of Hastelloy C-276 after the boriding treatment, typical 3D wear track profiles of the untreated and borided samples were obtained from the tests carried out at 20 N (Figure 8). It is obvious that the boriding process significantly reduced the wear track dimensions (Table IV). Also, the volume loss values automatically obtained by 3D profilometry (1750×10^3 mm^3 for untreated and 22 to 57×10^{-3} mm^3 for borided C-276)

were consistent with those calculated using 2D profilometry (Table IV).

D. Wear Mechanism and Surface Morphology

Top and cross-sectional views of the worn surfaces of the untreated and borided samples obtained at loads of 5, 10, and 20 N were analyzed to determine worn surface morphologies and operational wear mechanisms using $1000 \times$ and $5000 \times$ magnifications (Figures 9, 10,

Sample	Region	P_{max} (μN)	A (nm^2)	h_{max} (nm)	E_r (GPa)	H (GPa)
975 °C-5 h	boride layer	10,068.4 ± 0.3	387,791 ± 24,447	149.2 ± 4.1	256.4 ± 8.8	26.0 ± 1.6
	diffusion layer	10,073.3 ± 0.6	1,124,245 ± 88,567	224.2 ± 8.3	200.9 ± 8.1	9.1 ± 0.7
	substrate	10,076.2 ± 0.1	1,655,742 ± 12,297	270.4 ± 0.1	159.9 ± 5.0	6.1 ± 0.1
975 °C-7 h	boride layer	10,067.1 ± 0.1	411,109 ± 10,325	155.6 ± 2.7	233.0 ± 9.0	24.5 ± 0.6
	diffusion layer	10,072.8 ± 0.3	1,169,987 ± 49,446	231.8 ± 5.5	178.7 ± 8.5	8.6 ± 0.7
	substrate	10,076.1 ± 0.2	1,711,479 ± 18,372	279.2 ± 2.1	137.4 ± 6.9	5.9 ± 0.8

P_{max} is the maximum applied load, A is the projected area of the indenter on the boride layer, h_{max} is the maximum contact depth, E_r is the reduced elastic modulus and H is the hardness.

Table IV.   Average Surface Roughness, Mean COF, Wear Track Width and Depth, Volume Loss, and Wear Rate of the Untreated and Borided Hastelloy C-276 Samples Which Were Subjected to Reciprocating Wear Tests in Dry-Sliding Conditions (Mean ± SD, n ≥ 3)

Material	Load (N)	R_a (μm)	COF	Wear Track Width (μm)	Wear Track Depth (μm)	Volume Loss (10^{-3}mm^3)	Wear Rate 10^{-5}mm^3/Nm
Untreated	5	0.434 ± 0.034	0.613 ± 0.009	1804 ± 39	58.1 ± 7.3	943 ± 146	59.23 ± 9.16
975 °C-5 h		0.372 ± 0.199	0.468 ± 0.048	477 ± 23	1.8 ± 0.3	12 ± 5	0.75 ± 0.32
975 °C-7 h		0.435 ± 0.086	0.452 ± 0.060	497 ± 4	3.0 ± 0.6	23 ± 7	1.47 ± 0.46
Untreated	10	0.484 ± 0.055	0.587 ± 0.045	2202 ± 28	75.3 ± 6.9	1310 ± 264	44.73 ± 9.01
975 °C-5 h		0.319 ± 0.155	0.432 ± 0.033	538 ± 31	2.4 ± 0.7	14 ± 3	0.48 ± 0.12
975 °C-7 h		0.422 ± 0.048	0.431 ± 0.035	516 ± 17	3.3 ± 0.4	23 ± 7	0.77 ± 0.23
Untreated	20	0.515 ± 0.085	0.475 ± 0.005	2559 ± 46	92.6 ± 2.7	1909 ± 124	32.59 ± 2.12
975 °C-5 h		0.206 ± 0.123	0.416 ± 0.050	545 ± 36	7.9 ± 4.1	52 ± 22	0.89 ± 0.37
975 °C-7 h		0.260 ± 0.044	0.352 ± 0.027	584 ± 29	6.1 ± 2.0	32 ± 11	0.55 ± 0.19
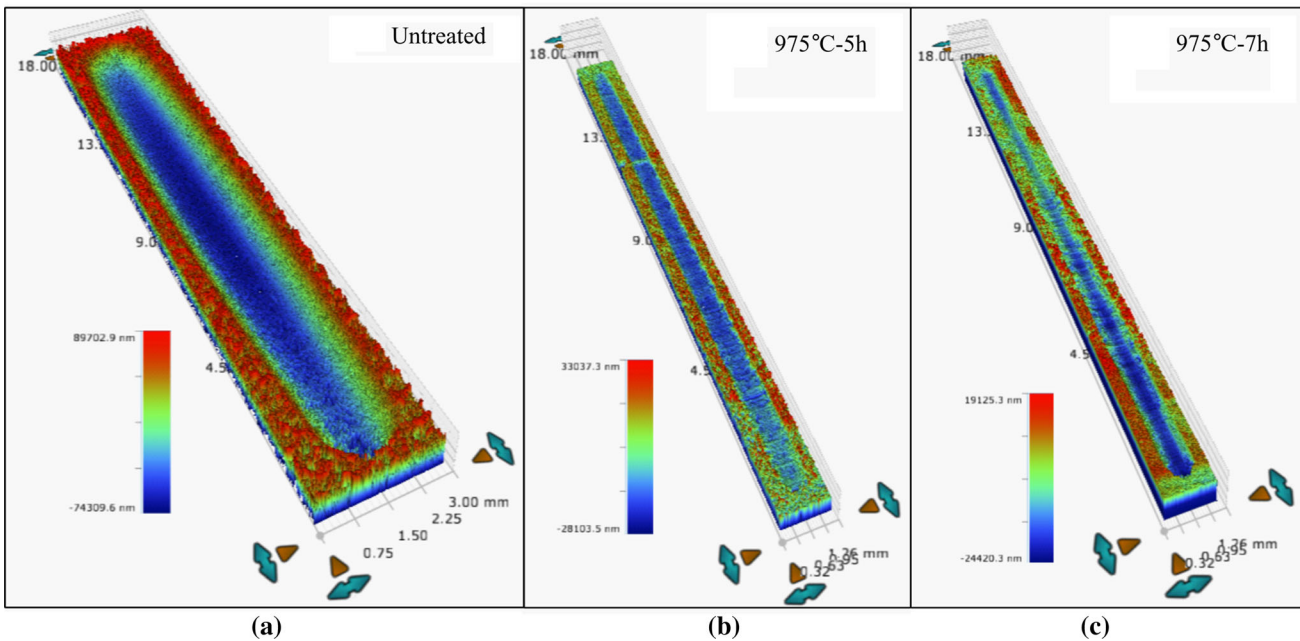
Fig. 8—3D wear track views of (a) untreated, (b) borided at 975 °C for 5 h, and (c) 7 h at 20 N. A variation of the color indicates the depth change in the wear track (Color figure online).

and 11). SEM images of the wear tracks obtained from the untreated specimens exhibit abundant parallel grooves or scratches along the sliding direction (Figure 9), attributed to the lower hardness of the untreated surfaces.[59,60] These grooves are mainly due to the plowing of micro-asperities that occurred during the wear tests. Smaller portions of micro-pits were also observed on the worn surfaces, especially at increased applied loads (Figure 9c). Fatigue cracks perpendicular to the sliding direction were formed due to the repetitive

Fig. 9—SEM images and EDS analysis of untreated Hastelloy C-276 worn at (*a*) 5 N, (*b*) 10 N, and (*c*) 20 N. (1) and (2) represent top and cross-sectional views of the worn surfaces, respectively.

loads experienced during the wear experiments, which triggered plastic deformation mechanisms.[61,62] The plastic deformation observed on the substrate surface was caused by the destructive action of the alumina counterpart,[5] which was more evident at higher applied loads. SEM and EDS analyses found discontinuous oxide islands, and accumulation of wear debris and grooves, which indicates abrasive wear, adhesion, and plastic deformation as the dominant wear mechanisms.

Additionally, the cross-sectional views of the wear tracks distinguish the wear-affected and wear-free layers, and the oxygen level was detected to be higher in the wear-affected zone by EDS spectra.

The wear morphologies of the borided samples (Figures 10 and 11) were different from those of the untreated samples. The high hardness of the borides provided better wear resistance. The presence of delamination craters and particle debris at a few regions was
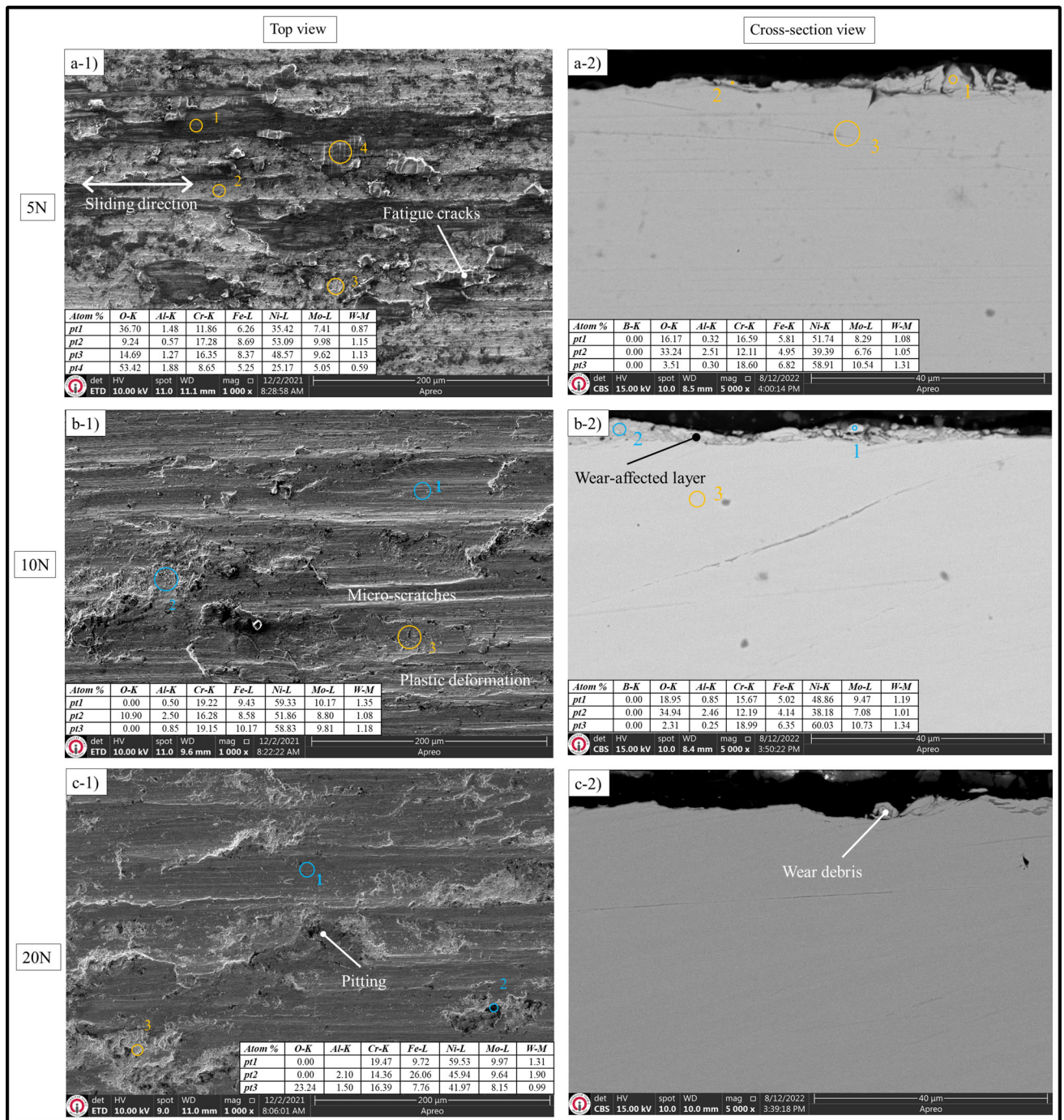
Fig. 10—SEM images and EDS analysis of 975 °C-5 h worn at (*a*) 5 N, (*b*) 10 N, and (*c*) 20 N. (1) and (2) represent top and cross-sectional views of the worn surfaces, respectively.

observed, which is an indication of an abrasive wear mechanism. Local ruptures and detachments seen in some regions are ascribed to cracks in the borides. Moreover, the boride layers are composed of a remarkable amount of oxygen, suggesting the formation of a tribo-oxide layer (also known as the glazed layer)[55,63] in dark regions of the SEM images. This layer is formed due to the increase in contact temperature during the wear tests, thought to be responsible for minimizing

wear rate and friction coefficients.[7] Therefore, abrasion, delamination, and oxidation wear mechanisms govern the wear process in the borided C-276 samples.[63]

The wear-affected boride layer, wear-free boride layer, diffusion layer, and substrate can be seen from the cross-sectional SEM micrographs of the wear tracks of the borided specimens (Figures 10 and 11). The EDS analysis exhibited a higher oxygen rate at the
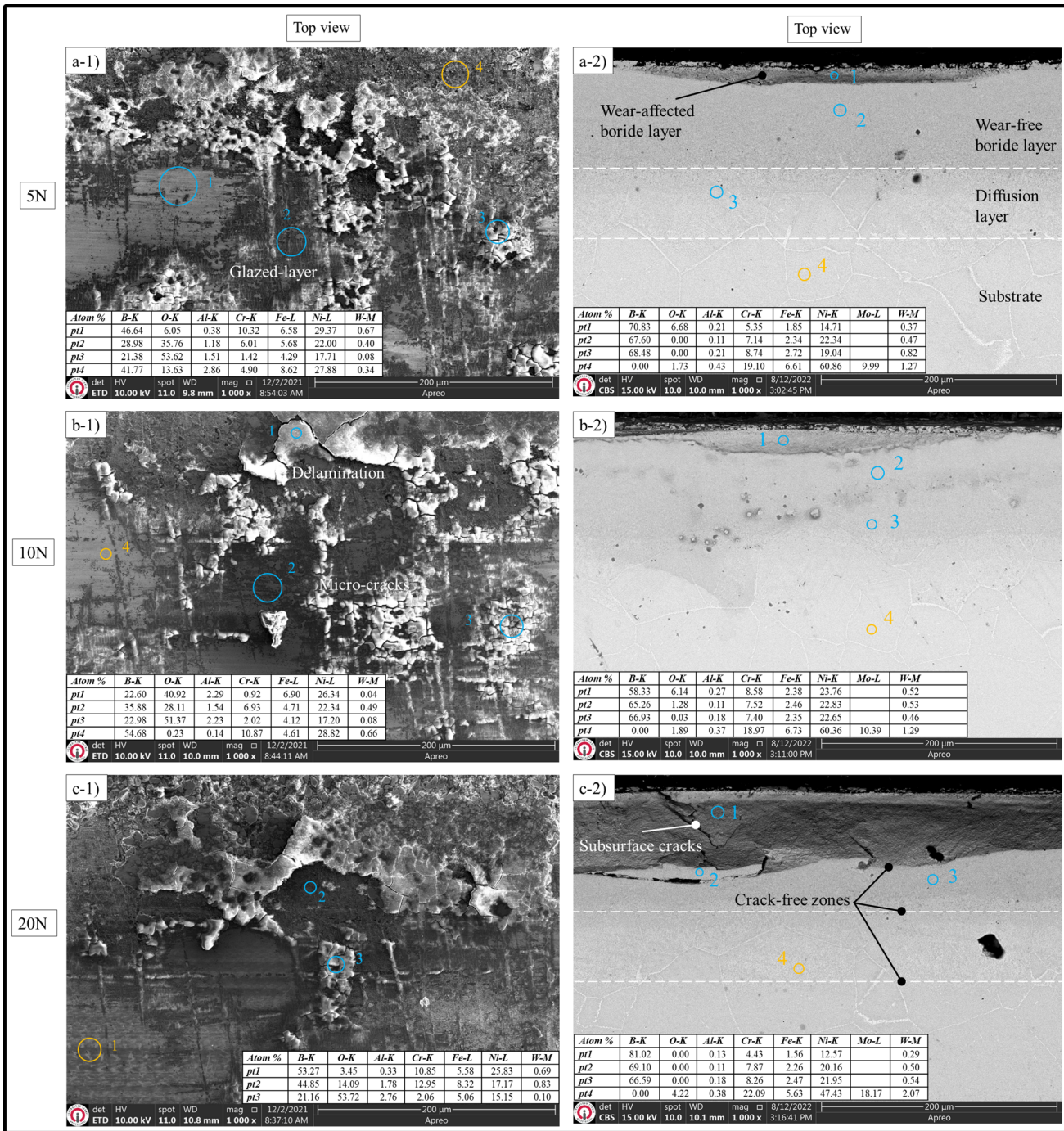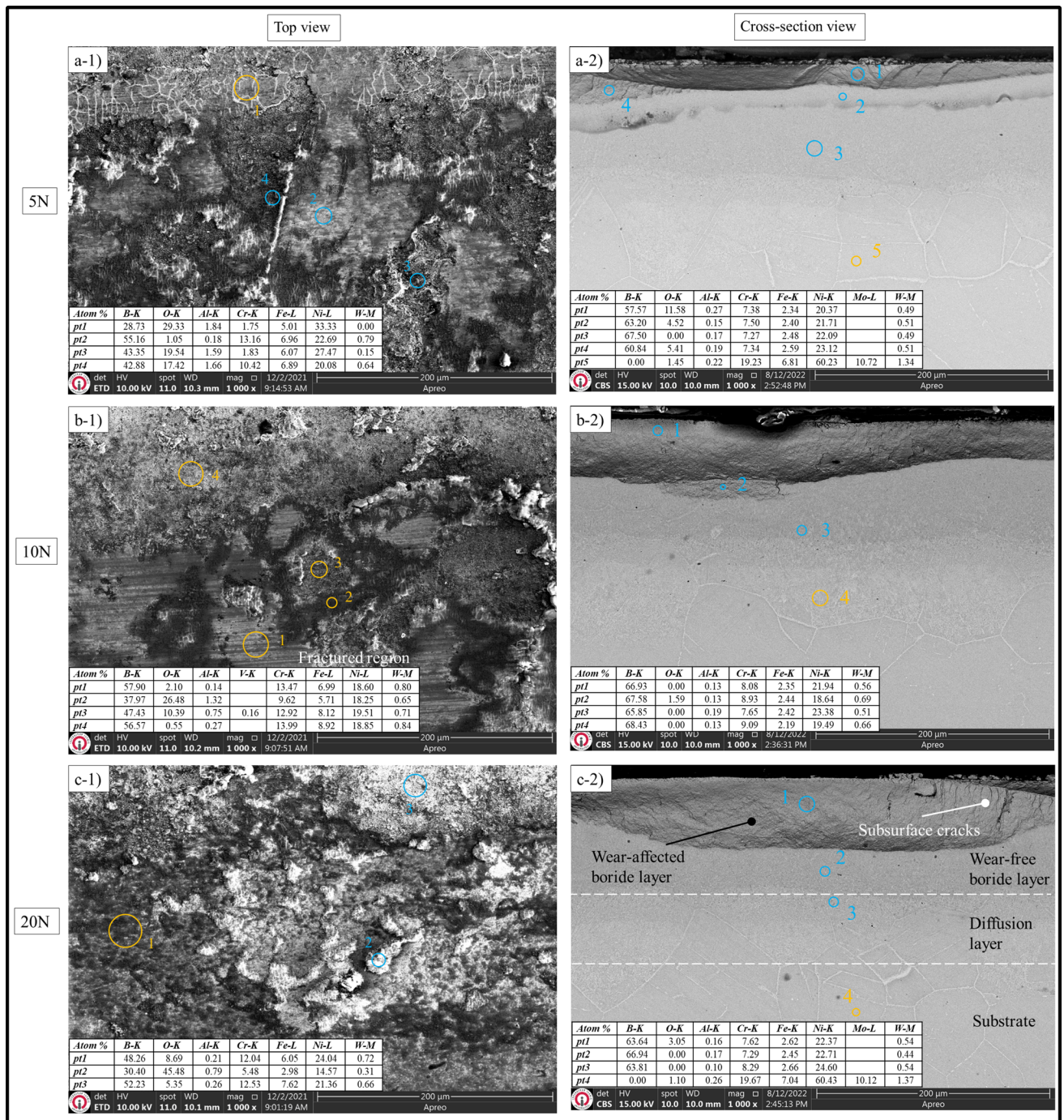
Fig. 11—SEM images and EDS analysis of 975 °C-7 h worn at (*a*) 5 N, (*b*) 10 N, and (*c*) 20 N. (1) and (2) represent top and cross-sectional views of the worn surfaces, respectively.

Panel a-1) — 5N, Top view

Atom %	B-K	O-K	Al-K	Cr-K	Fe-L	Ni-L	W-M
pt1	28.73	29.33	1.84	1.75	5.01	33.33	0.00
pt2	55.16	1.05	0.18	13.16	6.96	22.69	0.79
pt3	43.35	19.54	1.59	1.83	6.07	27.47	0.15
pt4	42.88	17.42	1.66	10.42	6.89	20.08	0.64

Panel a-2) — 5N, Cross-section view

Atom %	B-K	O-K	Al-K	Cr-K	Fe-K	Ni-K	Mo-L	W-M
pt1	57.57	11.58	0.27	7.38	2.34	20.37		0.49
pt2	63.20	4.52	0.15	7.50	2.40	21.71		0.51
pt3	67.50	0.00	0.17	7.27	2.48	22.09		0.49
pt4	60.84	5.41	0.19	7.34	2.59	23.12		0.51
pt5	0.00	1.45	0.22	19.23	6.81	60.23	10.72	1.34

Panel b-1) — 10N, Top view (Fractured region)

Atom %	B-K	O-K	Al-K	V-K	Cr-K	Fe-L	Ni-L	W-M
pt1	57.90	2.10	0.14		13.47	6.99	18.60	0.80
pt2	37.97	26.48	1.32		9.62	5.71	18.25	0.65
pt3	47.43	10.39	0.75	0.16	12.92	8.12	19.51	0.71
pt4	56.57	0.55	0.27		13.99	8.92	18.85	0.84

Panel b-2) — 10N, Cross-section view

Atom %	B-K	O-K	Al-K	Cr-K	Fe-K	Ni-K	W-M
pt1	66.93	0.00	0.13	8.08	2.35	21.94	0.56
pt2	67.58	1.59	0.13	8.93	2.44	18.64	0.69
pt3	65.85	0.00	0.19	7.65	2.42	23.38	0.51
pt4	68.43	0.00	0.13	9.09	2.19	19.49	0.66

Panel c-1) — 20N, Top view

Atom %	B-K	O-K	Al-K	Cr-K	Fe-L	Ni-L	W-M
pt1	48.26	8.69	0.21	12.04	6.05	24.04	0.72
pt2	30.40	45.48	0.79	5.48	2.98	14.57	0.31
pt3	52.23	5.35	0.26	12.53	7.62	21.36	0.66

Panel c-2) — 20N, Cross-section view

Atom %	B-K	O-K	Al-K	Cr-K	Fe-K	Ni-K	Mo-L	W-M
pt1	63.64	3.05	0.16	7.62	2.62	22.37		0.54
pt2	66.94	0.00	0.17	7.29	2.45	22.71		0.44
pt3	63.81	0.00	0.10	8.29	2.66	24.60		0.54
pt4	0.00	1.10	0.26	19.67	7.04	60.43	10.12	1.37

wear-affected layers, which indicates the growth of the oxides at the outermost boride layer. Also, subsurface cracks at the wear-affected zone are visible, especially at elevated loads (Figures 10(c-2) and 11(c-2)). It is worth mentioning that the regions between the wear-affected and wear-free layers, between the wear-free and diffusion layers, and between the diffusion layer and the substrate are crack free. This finding supports the effectiveness of the borides at given test conditions. The point EDS mapping of the borided samples found Ni, Cr, Mo, Fe, and W in the wear traces (Figures 10 and 11), which are present in the chemical composition of

Hastelloy C-276. B element was also detected in EDS spectra, which proves that the borides act as a protective layer in improving the wear resistance of Ni-based Hastelloy C-276.[7] The presence of higher aluminum elemental ratio is noted in the wear traces of the borided samples compared with untreated C-276. This indicates the occurrence of more element transfer from the abrasive ball to the untreated surfaces owing to their high wear resistance.

Using the SEM images, the wear track widths of the untreated specimens were measured as 1804 μm at 5 N, 2202 μm at 10 N, and 2559 μm at 20 N. The boriding process enabled the reduction of wear track width of the C-276 superalloy by approximately 75 pct (487 μm at 5 N, 527 μm at 10 N, and 564 μm at 20 N). No considerable difference was found between the boriding durations (5 and 7 hours). Wear scar width increased by pct22 and 10 pct when the applied load increased from 5 to 10 N for untreated and borided C-276, respectively. The increment was observed to be 42 pct and 18 pct as the load was further increased to 20 N. The widths of the wear traces measured by SEM are compatible with 2D- and 3D-surface profilometry results (Figures 6 and 8). Moreover, greater average volume loss and specific wear rate were obtained in untreated C-276 (Figure 7), which are in agreement with SEM results.

IV. CONCLUSIONS

In the current study, the boriding process was applied on Ni-based Hastelloy C-276 superalloy at 975 °C for 5 and 7 hours. The effects of the boriding treatment on the microstructural and tribological performance were assessed. The conclusions obtained from the results are summarized as follows:

1   Following the boriding process performed at 975 °C for 5 and 7 hours, boride layers that were crack, porosity, and silicide free, and also stable/continuous along the surfaces (even at the corners) were obtained.
2   The use of Si-free boron powder mixture prevented the growth of the nickel-silicide layer. The thickness and hardness of the coatings were observed to be 86.5 to 132.7 μm and 2016 to 2210 $HV_{0.1}$, respectively.
3   An increase in the treatment duration from 5 to 7 hours led to a 53 pct increase in boride thickness and a 10 pct increase in hardness.
4   XRD analysis determined Ni_2B as the dominant phase in addition to CrB, MoB_2, and Fe_2B phases in low rates at the coating layers grown in both boriding durations (5 and 7 hours).
5   The R_a values obtained from the untreated samples (0.601 μm) either decreased (0.537 μm for 5 hours) or increased (0.948 μm for 7 hours) after the boriding process. The R_a values of all samples decreased after wear testing. Increasing the applied load further decreased the R_a of the borided samples while increasing that of the untreated samples.
6   Due to the lubricating effect of the boride phases, the borided samples exhibited COF values which were 13 to 27 pct lower, depending on the wear conditions. It was observed that the COF was lower at higher loads in both the untreated and borided samples.
7   High surface hardness of the borides (2016 to 2210 $HV_{0.1}$) relative to the substrate (250 $HV_{0.1}$) was effective in reducing the wear rates of Hastelloy C-276. Boriding process enabled 44 to 67 times superior wear resistance at various applied loads. In the borided samples tested at a higher applied load (20 N compared with 5 N), the volume loss was 1.3-fold larger while the specific wear rate was 35 pct smaller.
8   The dominant wear mechanism of the untreated samples was abrasive wear and plastic deformation while that of the borided samples was oxidation-assisted delamination.
9   There was no material transfer from the abrasive ball to the articulating surfaces of the untreated samples. Conversely, Al was detected on the surfaces of the borided samples as high-hardness boride layers led to some damage on the abrasive ball.
10 The wear resistance of Hastelloy C-276 superalloy is not satisfactory due to its relatively low surface hardness, which can be improved by the boriding process, thereby enhancing the service life of the superalloy.

CONFLICT OF INTEREST

The authors declare that they have no known competing financial interests or personal relationships that could have appeared to influence the work reported in this paper.

REFERENCES

1. W. Fichtl: *Mater. Des.*, 1981, vol. 2, pp. 276–86.
2. E. Hernández-Sánchez, J.C. Velázquez, J.L. Castrejón-Flores, A. Chino-Ulloa, I.P.T. Avila, R. Carrera-Espinoza, J.A. Yescas-Hernández, and C. Orozco-Alvarez: *Mater. Trans.*, 2019, vol. 60, pp. 156–64.
3. I. Campos-Silva, A.D. Contla-Pacheco, A. Ruiz-Rios, J. Martínez-Trinidad, G. Rodríguez-Castro, A. Meneses-Amador, and W.D. Wong-Angel: *Surf. Coat. Technol.*, 2018, vol. 349, pp. 917–27.

4. N. Makuch, M. Kulka, P. Dziarski, and S. Taktak: *Surf. Coat. Technol.*, 2019, vol. 367, pp. 187–202.
5. D.W. Deng, C.G. Wang, Q.Q. Liu, and T.T. Niu: *Trans. Non-ferrous Met. Soc. China*, 2015, vol. 25, pp. 437–43.
6. D.C. Lou, J.K. Solberg, O.M. Akselsen, and N. Dahl: *Mater. Chem. Phys.*, 2009, vol. 115, pp. 239–44.
7. A.K. Rai, C.P. Paul, G.K. Mishra, R. Singh, S.K. Rai, and K.S. Bindra: *J. Mater. Process. Technol.*, 2021, vol. 298, 117298.
8. M. Kukliński, A. Bartkowska, D. Przestacki, and G. Kinal: *Materials*, 2020, vol. 13, p. 24.
9. M. Kulka, P. Dziarski, N. Makuch, A. Piasecki, and A. Miklaszewski: *Appl. Surf. Sci.*, 2013, vol. 284, pp. 757–71.
10. N. Makuch, M. Kulka, and A. Piasecki: *Surf. Coat. Technol.*, 2015, vol. 276, pp. 440–55.
11. A. Günen, K.M. Döleker, M.E. Korkmaz, M.S. Gök, and A. Erdogan: *Surf. Coat. Technol.*, 2021, vol. 409, 126906.
12. A. Günen: *Metall. Mater. Trans. A.*, 2020, vol. 51A, pp. 927–39.
13. A.D. Contla-Pacheco, M. Keddam, L. Lartundo-Rojas, M. Ortega-Avilés, I. Mejía-Caballero, and I. Campos-Silva: *Surf. Coat. Technol.*, 2021, vol. 420, 127355.
14. A.P. Krelling, F.S. Melo, E.A.S. Almeida, C.E. da Costa, and J.C.G. Milan: *Mater. Res. Exp.*, 2019, vol. 6, p. 106410.
15. I. Campos-Silva, A.D. Contla-Pacheco, U. Figueroa-López, J. Martínez-Trinidad, A. Garduño-Alva, and M. Ortega-Avilés: *Surf. Coat. Technol.*, 2019, vol. 378, 124862.
16. T. Lindner, M. Löbel, R. Hunger, R. Berger, and T. Lampke: *Surf. Coat. Technol.*, 2020, vol. 404, 126456.
17. I. Akande, O. Oluwole, O. Fayomi, and O. Odunlami: *Mater. Today*, 2021, vol. 43, pp. 2222–31.
18. T.C. Chen, C.C. Chou, T.Y. Yung, R.F. Cai, J.Y. Huang, and Y.C. Yang: *Surf. Coat. Technol.*, 2020, vol. 385, 125442.
19. T.M. Pollock and S. Tin: *J. Propul. Power*, 2006, vol. 22, pp. 361–74.
20. J. Li, Y. Lu, H. Zhang, and L. Xin: *Tribol. Int.*, 2015, vol. 81, pp. 215–22.
21. J.Y. Yun, H.S. Lee, D.H. Hur, W.S. Kang, C.H. Bae, and S.J. Kim: *Wear*, 2016, vol. 368–369, pp. 344–49.
22. A. Günen, E. Kanca, H. Çakir, M.S. Karakaş, M.S. Gök, Y. Küçük, and M. Demir: *Surf. Coat. Technol.*, 2017, vol. 311, pp. 374–82.
23. Y. Kayalı, E. Kanca, and A. Günen: *Mater. Charact.*, 2022, vol. 191, 112155.
24. V. Sista, O. Kahvecioglu, G. Kartal, Q.Z. Zeng, J.H. Kim, O.L. Eryilmaz, and A. Erdemir: *Surf. Coat. Technol.*, 2013, vol. 215, pp. 452–59.
25. A. Günen and E. Kanca: *Pamukkale Univ. J. Eng. Sci.*, 2017, vol. 23, pp. 411–16.
26. M. Hashim, K.E. SarathRaghavendraBabu, M. Duraiselvam, and H. Natu: *Mater. Des.*, 2013, vol. 46, pp. 546–51.
27. W.C. Oliver and G.M. Pharr: *J. Mater. Res.*, 1992, vol. 7, pp. 1564–83.
28. Y.T. Cheng and C.M. Cheng: *Surf. Coat. Technol.*, 2000, vol. 133–134, pp. 417–24.
29. S.J. Bull: *J. Phys. D Appl. Phys.*, 2005, vol. 38, pp. R393-413.
30. W.C. Oliver and G.M. Pharr: *J. Mater. Res.*, 2004, vol. 19, pp. 3–20.
31. Y. Kanca, P. Milner, D. Dini, and A.A. Amis: *J. Mech. Behav. Biomed. Mater.*, 2018, vol. 78, pp. 36–45.
32. E.A. Eid, M.M. Sadawy, and A.M. Reda: *Mater. Chem. Phys.*, 2022, vol. 277, 125446.
33. K. Holmberg and A. Matthews: *Coatings tribology: properties, mechanisms, techniques and applications in surface engineering*, Elsevier, Amsterdam, 2009.
34. I.J. McColm: *Ceramic Hardness*, Springer, New York, 2013.
35. N. Makuch and M. Kulka: *Ceram. Int.*, 2016, vol. 42, pp. 3275–89.
36. I. Campos-Silva, M. Ortiz-Domínguez, O. Bravo-Bárcenas, M.A. Doñu-Ruiz, D. Bravo-Bárcenas, C. Tapia-Quintero, and M.Y. Jiménez-Reyes: *Surf. Coat. Technol.*, 2010, vol. 205, pp. 403–12.
37. W.D. Callister and D.G. Rethwisch: *Materials Science and Engineering: An Introduction*, Wiley, New York, 2018.
38. S. Anandh Jesuraj, P. Kuppusami, S. Ajith Kumar, P. Panda, and S. Udaiyappan: *Mater. Chem. Phys.*, 2019, vol. 236, p. 121789.
39. S. Turgut and A. Günen: *J. Mater. Eng. Perform.*, 2020, vol. 29, pp. 6997–7010.
40. B. Kurt, L. Özdoğan, B. Güney, Ö.S. Bölükbaşı, and A. Günen: *Surf. Coat. Technol.*, 2020, vol. 385, 125332.
41. G.Z. Voyiadjis and M. Yaghoobi: *Crystals*, 2017, vol. 7, p. 321.
42. G. Deng, A.K. Tieu, X. Lan, L. Su, L. Wang, Q. Zhu, and H. Zhu: *Tribol. Int.*, 2020, vol. 144, 106116.
43. M.A. Chowdhury, M.K. Khalil, D.M. Nuruzzaman, and M.L. Rahaman: *Int. J. Mech. Mechatron. Eng.*, 2011, vol. 11, pp. 45–49.
44. S.R. Schmid and L.G. Hector: *Macroscale Insight from Nanoscale Testing*, Springer, Nanotribology, 2003, pp. 399–410.
45. S.R. Schmid and L.G. Hector: *Nanotribology*, 2002, vol. 1, p. 399.
46. B.J. Babalola, S. Salifu, and P.A. Olubambi: *J. Mater. Eng. Perform.*, 2020, vol. 29, pp. 8348–58.
47. L. Li, K. He, S. Sun, W. Yang, Z. Yue, and H. Wan: *Tribol. Lett.*, 2020, vol. 68, p. 26.
48. C.N. Panagopoulos, K.I. Giannakopoulos, and V. Saltas: *Mater. Lett.*, 2003, vol. 57, pp. 4611–16.
49. A.D. Sarkar: *Friction and wear*, Academic Press, New York, 1980.
50. E. Rabinowicz and R.I. Tanner: *J. Appl. Mech.*, 1966, vol. 33, p. 479.
51. A. Günen, B. Kurt, P. Milner, and M.S. Gök: *Int. J. Refract Metal Hard Mater.*, 2019, vol. 81, pp. 333–44.
52. E. Atar, E.S. Kayali, and H. Cimenoglu: *Surf. Coat. Technol.*, 2008, vol. 202, pp. 4583–90.
53. H. Cimenoglu, E. Atar, and A. Motallebzadeh: *Wear*, 2014, vol. 309, pp. 152–58.
54. E. Garcia-Bustos, M.A. Figueroa-Guadarrama, G.A. Rodríguez-Castro, O.A. Gómez-Vargas, E.A. Gallardo-Hernández, and I. Campos-Silva: *Surf. Coat. Technol.*, 2013, vol. 215, pp. 241–46.
55. M.S. Gök, Y. Küçük, A. Erdoğan, M. Öge, E. Kanca, and A. Günen: *Surf. Coat. Technol.*, 2017, vol. 328, pp. 54–62.
56. A. Kalyon, O. Palavar, and D. Özyürek: *J. Mater. Eng. Perform.*, 2019, vol. 28, pp. 2853–65.
57. Y. Gao and M. Zhou: *Appl. Sci.*, 2018, vol. 8, p. 12.
58. Y. Wang, S. Zhao, Z. Jia, J. Ji, D. Liu, T. Guo, and Y. Ding: *Adv. Mater. Sci. Eng.*, 2020, vol. 2020, p. 5453703.
59. A. Günen, M. Keddam, S. Alkan, A. Erdoğan, and M. Çetin: *Mater. Charact.*, 2022, vol. 186, 111778.
60. A.P. Krelling, C.E. da Costa, J.C.G. Milan, and E.A.S. Almeida: *Tribol. Int.*, 2017, vol. 111, pp. 234–42.
61. X. Song, L. Wang, M. Niinomi, M. Nakai, and Y. Liu: *Mater. Sci. Eng., A*, 2015, vol. 640, pp. 154–64.
62. N.B. Pugacheva, T.M. Bykova, and L.M. Zamaraev: *Phys. Met. Metall.*, 2020, vol. 121, pp. 590–96.
63. A. Günen, E. Kanca, M.S. Karakaş, V. Koç, M.S. Gök, Y. Kanca, A. Çürük, and M. Demir: *Surf. Coat. Technol.*, 2018, vol. 348, pp. 130–41.